Deep Spectral Convolution Neural Network Based Leukemia Cancer Detection Using Invariant Entity Scalar Feature Selection

B. Divyapreethi [1,*], A. Mohanarathinam [2]
[1]Research scholar, Department of Electronics Communication Engineering,
[2]Associate professor, Department of Biomedical Engineering,
Faculty of Engineering, Karpagam Academy of Higher Education, Coimbatore.
Emails: mohanarathinam@gmail.com; divisathvi@gmail.com

Abstract

Leukemia, a cancer that attacks human white blood cells, is one of the deadliest illnesses. Detecting affected cells in microscopic images becomes tedious because feature variants are not predicted correctly by a hematologist. Therefore image handling techniques failed to select the importance of the features scaling counts, entities, and precise size and shape of cells presented in the microscopic image. To resolve this problem, Deep Spectral Convolution Neural Network (DSCNN) based on Leukemia cancer detection using Invariant Entity Scalar Feature Selection (IESFS) is proposed to identify the risk factor of cancer for early diagnosis. Initially, preprocessing is carried out using cascade Gabor filters. Based on Structural Cascade Segmentation (SCS), the white blood cell regions are categorized into affected and non-affected margins and verify the edges using canny edge mapping. This estimates the scaling cell size, counts, entities and angular cell projection of weights from each segmented feature region. Then find the entity relation of cell projection equivalence using Color Intensive Histogram Equalization (CIHE). After segmenting the angular vector, projection scaling is applied to correlate the entity's object scaling comparator. Then scaling features were selected using Invariant Entity Scalar Feature Selection (IESFS) by averaging the mean depth values of feature weight and trained with a deep convolution neural network for predicting max equivalence entity weights for finding the affected cells and counts in microscopic images. This improves the prediction of cancer cell accuracy as well high performance in sensitivity 92.7 %, specificity 92.3 %, and f-measure 93.6 % with redundant time complexity.

Keywords: Leukemia Cancer Detection: Feature selection and classification: Structural Cascade Segmentation: CNN: Histogram Equalization.

1. Introduction

Developing medical image analysis, leukaemia cancer disease identification is one of the most promising research projects in the recent medical field for early diagnosis [1]. Leukaemia is cancer in the blood cells that contains many white blood cells damages, which are immature cells that impede the function of other blood components, primarily platelets and red blood cells. To treat this type of cancer and all types of cancer, it is essential to diagnose it early based on image analytics modes [2]. It takes more time and effort to perform the diagnostic procedure manually by a technician and is more cost-effective with the help of the equipment process. By examining micro-imaging, researchers have created a number of methods for machine learning-based leukaemia diagnosis [3]. In this paper, an automated leukaemia detection method is presented. In the manual method of diagnosing leukaemia, experts examine microscopic images. It is a laborious and time-consuming procedure that is inconsistently accurate and dependent on individual skills [4]. One of the most

Doi : https://doi.org/10.54216/JCIM.140203
Received: January 19, 2024 Revised: March 01, 2024 Accepted: June 07, 2024

widely used techniques is the Deep neural network. This research intends a Convolutional Neural Network (CNN) based on feature selection and classification.

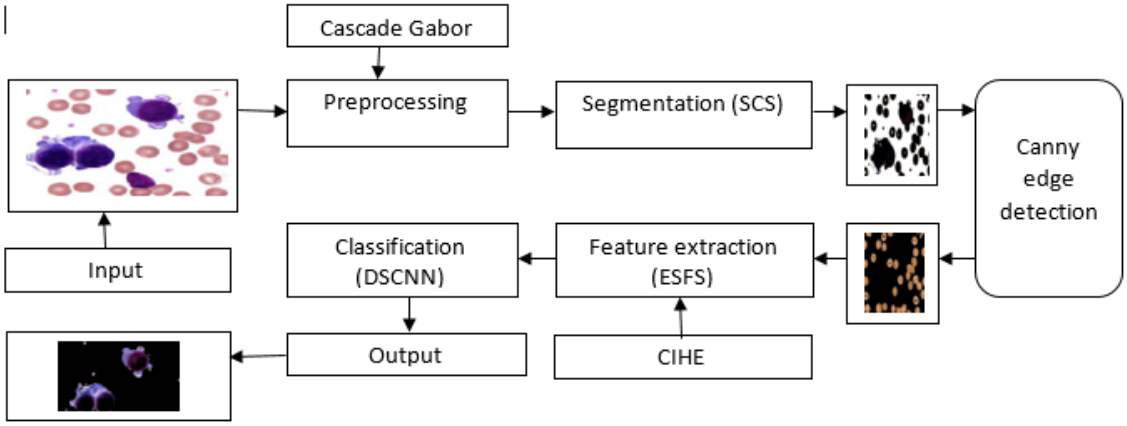

Figure 1: Overall Proposed architecture Diagram

Deep Neural networks are the method of choice as a classification tool because they are a well-known technique as a successful classifier in many real-world applications. They select the best features to classify the results [5]. The training and verification process is one of the critical steps in creating an accurate process model using CNN. The image is analyzed based on segment cell variation in the research area. The weights of the lymphocytic features are constantly updated until related entity levels identify the cancer cells effectively. The scope of the research is to improve leukaemia cancer disease detection in microscopic images in high determination imaging.

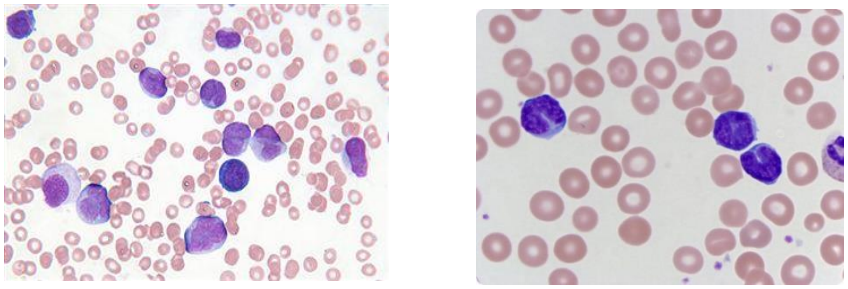

Figure 2: Microscopic collective samples

This highly supports identifying the patients' risk based on the optimized features selection and classification. This can improve the medical imaging analysis based on an in-depth feature neural network by detecting the cancer cell by evolving high precision, recall rate in classification accuracy produce best detection and support for medical healthcare cancer treatment. This supports automatic detection and risk of the cancer level to support early risk prediction and diagnosis with redundant time. The study's main objective is to enhance Leukemia cancer detection in microscopic images using an optimized deep neural network. To improve the feature selection and classification based on effectively identifying cancer cell scaling factors. Implement a structural cascade segmentation (SCS) to split the variant and non-variant cancer cells effectively optimized with canny edge mapping. In order to identify a salient set of features that can be utilized to predict an impacted cell as normal or concerned cells, an invariant entity scalar feature selection technique is intended. Adaptive deep convolution neural classier was applied to categorize cancer risk levels by class by reference. To improve the cancer detection accuracy in precision rate, recall rate, F-measure, false reduction and low time complexity.

Doi : https://doi.org/10.54216/JCIM.140203
Received: January 19, 2024 Revised: March 01, 2024 Accepted: June 07, 2024

The relevant work completed by different authors is covered in the remainder of section 2. Section 3 explains how to implement the suggested system. Section 4 presents the findings and the arguments made to support them, while Section 5 wraps up the suggested approach.

2. Related work

Automated leukaemia detection systems overcome these shortcomings by analyzing microscopic images [6, 7]. It extracts the necessary parts of the image and applies some filtering techniques. K-means clustering method was used for leukocyte detection. Histogram equalization and the Jax algorithm were applied to the leukocyte group [8]. Calculate features like mean, standard deviation, colour, area, and circumference to detect leukaemia. Because of high dimension cascades, non-illumination in microscopic pictures results in redundant accuracy [9]. When determining leukaemia cell counts, some invariant image features become non-determinant due to noise ratio impulsiveness caused by poor contrast. Due to the discovery of a component that increases cell destruction and affects the angle of affection, segmentation and edge mapping in WBC scalar characteristics remain poorly understood [10]. Because regressive cells are hard to forecast, increasing entity relation fragmentation is non-regulatory and leads to intend self-occlusion[11]. Due to non-scaling features, the classification doesn't produce match case label reduction, leading to low-level accuracy in precision, recall, F-measure and more time complexity [12].

Due to changes in skin and impression conditions, some noise is introduced, and image quality is compromised [13], which can result in false details while ignoring accurate details. Therefore, the optimization algorithm should minimize the effect of incorrect information and maximize FMR (False Match Rate) and FNMR (False Mismatch Rate). There are a couple of picture division techniques: region-based, bunch-based, limit-based, and watershed-based picture division [16, 17]. Clinical picture division is essential in clinical applications for early findings and conspicuous evidence of disease states [18]. Deep vector Convolutional Neural Networks (DVCNNs) are the most ordinarily involved picture division procedures in PC vision [19, 20]. CNN profoundly views clinical picture examination. A CNN utilizes AI classifiers. The author continues to use the Dense Convolutional Neural Network (DCNN) algorithm for automatic WBC detection from images of tiny blood cells [21]. However, image segmentation and pre-processing were not the main emphasis of that study, thus further work is needed to forecast the outcomes

.

In order to automatically diagnose leukemia cancer, the survey's main focus is on microscopic blood cell image segmentation [22, 23]. Comprehensive picture segmentation techniques like region-based and clustering-based segmentation are presented by the author [5]. Using flow cytometry (FC) technology, the author investigates the use of the Bayesian-based Infinite Gaussian Mixtures (BIGM) method for the automatic diagnosis of ALM [24]. However, the system is unable to produce precise findings regarding AML illness. The colour space transformation technique used to anticipate and extract WBC from minuscule images is presented by the author [25]. In a similar vein, the author diagnoses leukemia cancer using tiny images and statistical measures like mean and standard deviation. However, using that method takes more time. The classification of leukaemia cancer is done by the author using K-Nearest Neighbor (KNN), Neural Network (NN), and Support Vector Machine (SVM) [26]. Similarly, utilizing microscopic pictures, an ANF (Adaptive Neuro-Fuzzy) approach for cancer prediction is effectively provided by the author [27]. However, those strategies did not yield results for categorization. The Gabor filtering technique is widely used in the object recognition research community for structure-based feature extraction. It is frequently used to patterns in faces, fingerprints, and facial expressions [28]. By suitably altering their filter size, gabor filters come in handy for detecting fringe orientations on both large and tiny fringe structures.

The image's content is characterized by a combination of colour, texture areas, and various shapes [29]. For this reason, we chose image feature extraction using dimensional Gabor filtering, a widely used shape and texture analysis tool. Gabor filters are also used in other image processing fields [30]. Once the edge direction is found, the missing pixel is interpolated into the matching kernel using the currently available kernel regression algorithm. Finding the approximate function at the sample locations with the least amount of error can be done using kernel regression.

Doi : https://doi.org/10.54216/JCIM.140203
Received: January 19, 2024 Revised: March 01, 2024 Accepted: June 07, 2024

3. Methodology

The development was carried out to process leukaemia cancer cells in microscopic images based on Deep Spectral Convolution Neural Network Based Leukemia Cancer Detection Using Invariant Entity Scalar Feature Selection. The intakes microscopic input images from the Medical repository and concentrates on feature selection and classification. The classification is carried out through marginal spectral values from feature dependencies by intending a soft-max logical activation function to predict the result and precision margin. The cascade sliding window-based Gabor filters are applied to filter noise from microscopic images, and Structural Cascade Segmentation (SCS) methods are used to segment the cells. To intent, canny edge mapping to identify the exact feature boundaries of leukaemia cells by concentration exactness of scaling cell size, counts, entities and angular cell projection of weights from each segmented feature region. Based on the segmented regions Color Intensive Histogram Equalization (CIHE) is applied to detect the variance of cell structure difference.

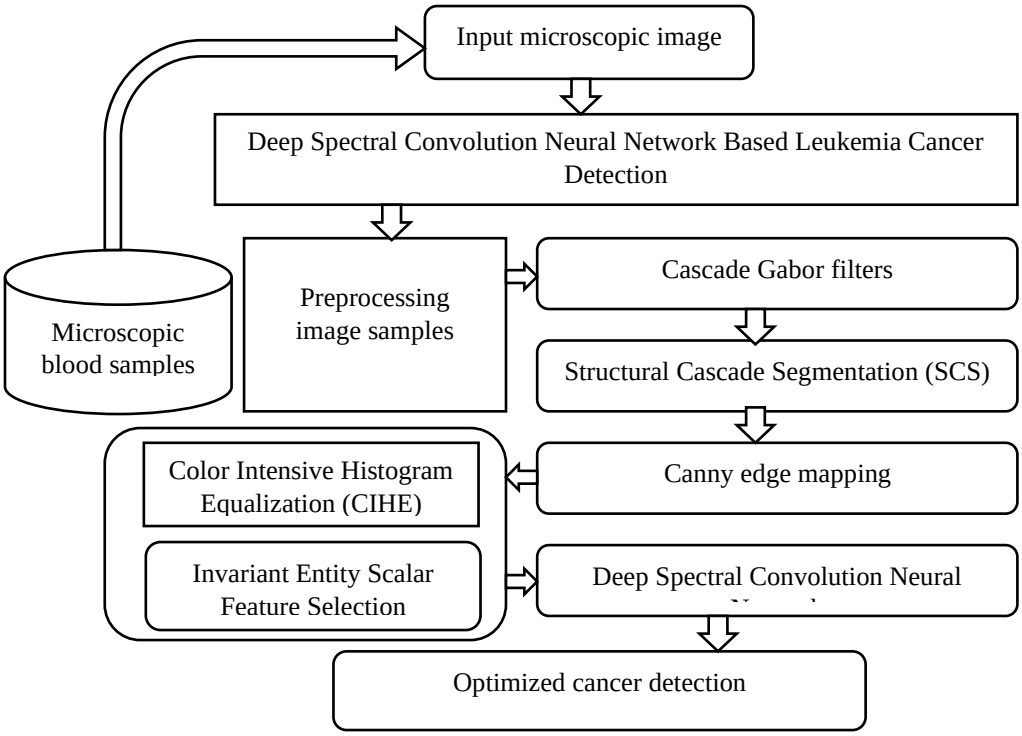

Figure 3: IESFS-DSCNN architecture

Together with the development of leukaemia identification, the features related to leukaemia cell dependencies were considered to analyze the feature weights. During the digital analysis, adaptive Gabor filters carried out the image enhancement to achieve high filtering to reduce the noise and get augmented segmentation. Figure 3 shows the Proposed Workflow Architecture IESFS-DSCNN. The segmentation enriches the boundary levels to identify the objects and improves the entities to predict the weights among the cell difference by applying the Probability distribution function to find the groom cell variations placed differently from the normalized cell to get the identified affected cells.

3.1. Preprocessing Image samples

Preprocessing was carried out to produce a noiseless image to enhance the degraded image. The biomedical images are from microscopic images taken from a digitalized image intensity level, so the fundamental entities of image features are illuminated less intensely to visualize the objects and entities in mages. So enhancement needs to remove the noise, resize, and restore pixels to contrast the image to improve the quality for higher analysis to get the accuracy.

Doi : https://doi.org/10.54216/JCIM.140203
Received: January 19, 2024 Revised: March 01, 2024 Accepted: June 07, 2024

A) Image stabilization

The microscopic images are degraded images that need to be enhanced before processing to select the features from the microscopic image. Because of microscopic cell type content, object content entities level margin to improve the edge detection segmentation through wiener filter. Utilizing the gradient filter's assistance, the image can be made smoother to improve edge preservation. To improve the image's quality, to minimize and stabilize it, Structured similarity position g, resize, PSNR, MSE, and RMSE were applied. The following equation is used to maximize the wiener's gradient optimization 'G'.

$$G = \frac{H}{|H|^2+1/SNR} \quad (1)$$

$$suppose, 1/SNR = k, G = \frac{H}{|H|^2+1/K} \quad (2)$$

Using the deteriorated conjugant function, "H" is stabilized in relation to the filter optimization in order to restore the degraded level. The Wiener filter with the above design filters the deteriorated image. The Gradient filter is applied after the Wiener filter has recovered the painting.

$$\nabla f = grad(f)\begin{bmatrix} gx \\ gy \end{bmatrix} = \begin{bmatrix} \partial f/\partial x \\ \partial f/\partial y \end{bmatrix} \quad (3)$$

Images are applied using gradient functions to remove noise from the previously mentioned equations 2 and 3. The image's magnitude is expressed as,

$$M(x,y) = mag(\nabla f) = \sqrt{gx^2 + gy^2} \quad (4)$$

To minimize noise, the edges derived from the nonlinear process are preserved a bilateral filter was used for optimization. In order to smooth out object presence in the microscopic image, this selects the neighboring pixels to contrast the image. Where M(x, y) comes from go and gy, the degraded functions, respectively, represents the gradient function's magnitude from the bilateral perspective.

$$bf(I)p = \frac{1}{W_p}\sum_{q\in N(p)} G\sigma s(\|P-Q\|)G\sigma r(\|I_p - I_q\|)I_q \quad (5)$$

$$W_p = \sum_{q\in N(p)} G\sigma s(\|P-Q\|)G\sigma r(|I_p - I_q|)I_q. \quad (6)$$

To evaluate the differential level of the object reference between Gσs, the Gaussian spatial distance, and Gσr, the Gaussian on the pixel, the linear retention in the Wp weight output to the Gaussian distance depends on the surrounding image pixel.

$$Si = \sum_j M_{ij}(I)P_j \quad (7)$$

$$M_{ij} = \frac{1}{|W|^2} \quad \sum_{K:(i,j)\in Wk} 1 + \frac{(I_i-U_k)(I_j-U_k)}{\sigma k^2+\epsilon} \quad (8)$$

When it comes to the 'I' guiding image, M_{ij} stood for the filter kernel, the preprocessed picture difference in dispute is shown by σ, and the Ki kernel sought to annihilate K at mean I in pixel. In order to improve the normalizing process' performance, this improves the quality of the noiseless image.

Doi : https://doi.org/10.54216/JCIM.140203
Received: January 19, 2024 Revised: March 01, 2024 Accepted: June 07, 2024

b) Cascade texture Filter

The Cascade Gabor texture filtering in image representation is the transformation of the image into Gabor kernels of the same family given by the formula, where Ix represents the image's grayscale distribution and gmn is the definition of the image's convolution with the Gabor kernel: G_{mn}(s, t). Where s and t are channel veil size factors, $gmn*$ is the mind-boggling form of the parent Gabor capability gmn, and Gmn is the convolution result comparable to the Gabor part. After applying the Gabor filter to images of various scales and orientations, obtain an array of scales.

$$E(m,n) = \sum_s \sum_t |G_{mn}(x,y)| \quad (9)$$

These amounts address how much energy at various sizes and directions in the picture. Texturing-based search primarily motivates tracking images or textures with comparative surfaces. Suppose images or regions with comparative textures. Thus, to address the homogeneous textural features of the area, utilize the extents of the change coefficients' mean (μmn) and standard deviation (σmn).

$$\mu_{mn} = \frac{E(m,n)}{PXQ} \quad (10)$$

$$\sigma_{mn} = \frac{\sqrt{\sum_x \sum_y (|G_{mn}(x,y)| - \mu_{mn})^2}}{PXQ} \quad (11)$$

A feature vector F (surface portrayal) is made utilizing μmn and σmn as the parts. The component vector, with M scopes and N directions employed in an identical style of execution, is provided by: Create a feature vector F (set representation) using μmn and σmn as feature elements. A typical implementation uses M criteria and N orientation. Given by the eigenvectors.

$$F_{texture} = (\mu_{00}, \sigma_{00}, \mu_{01}, \sigma_{01}, \dots\dots\dots\dots . \mu_{MN}, \sigma_{MN}) \quad (12)$$

Let Tq and Td be the surface vectors of the query images and the image in the data set separately, and characterize the Euclidean distance as the distance between two texture vectors meant by Dc(q,d).

$$D_c(q,d) = \sqrt{\sum_{i=1}^{48} (T_{qi} - T_{di})^2} \quad (13)$$

In order to determine whether the textural properties of the database picture d and the query image q are similar, recommend using Euclidean distance for simplification.

3.2 Structural cascade segmentation (SCS)

This algorithm created a slicing window on image pixels by cornering the object points accurately to enhance the affected region of leukaemia to segment separately. The segmentation is carried out to filter the cell along with the difference in variation in the object's boundary. This covers the entity resolution by improved edge smoothing based on the ridges. This enhances the boundary segmentation at the edges to extract the object entities with the features. Based on the orthogonal feature observation, the localized filter is smoothened to identify the counterpart of image cells to get the boundary region to extract the objects. This covers the cell difference by identifying the difference in pixel variation. Let us an object region cover$R = \cup_{n=-\infty}^{n=+\infty} [a_n, a_{n+1}]$. we define $P_n = a_{n+1} - a$ And $C_n = \frac{a_{n+1}+a_n}{2}$ around each and a neighbourhood of radius. Let a ramp function as:

$$\gamma(t) = \begin{cases} 0 & t \le -1 \\ 1 & t \ge 1 \end{cases} \quad (14)$$

Where $\gamma^2(t) + \gamma^2(-t) = 1, \forall t \in R$. Let b be a bump function $b_t = \gamma(t/\varepsilon)\gamma(-t/\varepsilon)$supported on $[-\varepsilon, \varepsilon]$be the window function supported on $\left[-\frac{P_n}{2} - \varepsilon \frac{P_n}{2} + \varepsilon\right]$

Doi : https://doi.org/10.54216/JCIM.140203
Received: January 19, 2024 Revised: March 01, 2024 Accepted: June 07, 2024

$$\omega_n(t) = \begin{cases} \gamma^2\left(\frac{t+{}^{P_n}/_2}{\varepsilon}\right) & if\ \ t\ \epsilon[p_n/2-\varepsilon, -p_n/2+\varepsilon] \\ 1 & if\ t\ \epsilon[-{}^{p_n}/_2-\varepsilon, {}^{p_n}/_2-\varepsilon] \\ \gamma^2\left(\frac{-t+P_n/2}{\varepsilon}\right) & if\ \ t\ \epsilon[p_n\ /\ 2-\varepsilon, p_n\ /\ 2+\varepsilon] \end{cases} \quad (15)$$

Representing the exponential boundary points ,$_n(t) = \frac{1}{\sqrt{P_n}} \exp\left(-2i\pi m \frac{t-a_n}{p_n}\right)$, the ridge boundary edges are covered by the cell margins in exponentially, $u_{m,n}$, where each $u_{m,n}$ is supported on $a_n - \varepsilon, a_{n+1} + \varepsilon$and is given by

$$u_{m,n}(t) = \omega_n(t-c_n)e_{m,n}(t) + b(t-a_n)e_{m,n}(2a_n t) - b(t-a_{n+1})e_{m,n}(2a_{n+1}-t) \quad (16)$$

Conversely, the boundary points are considered a sliding window for creating the object covering the region to iterate to segment to choose a small window size. The texture boundaries are preserved to create best-case local texture areas. If the scope of this window varies with regional features, that is, in a smooth space, the measure will be more considerable; In the dynamic area, the window size is smaller in image cells and be covered with cell difference in variance to make count difference cells. In this proper enhanced boundary region segmentation, the cornered edges are sharpened into seed the intensity of the cell by initiated difference level. by supporting microscopic image, the fusion levels are differentiated by accurately counting the affected and non-affected difference.

3.3 Color Intensive Histogram Equalization (CIHE)

This selects the Intensive features to depend on colour variation between a normal cell and leukaemia cells on each segmented part. In this stage, the histogram equalization is processed to identify the difference between the damaged cells based on the Threshold values 'T'. Initially, the Threshold is determined to find the Probability Distribution Function (PDF). Then the differentiation is carried out to handle cell differentiation h(x, y). Let the preprocessing image p' at the histogram process be defined as p(h)→h(x, y) to attain microscopic image 0 ≤ x ≤ L-1. Based on the neighbour pixel difference, the fluctuation gives the empty regions at cell counts to make object entity correlation at the edge level. So the equalization is carried about cell difference level. The equalization behind the process, the cell difference is filtered by histogram variant weights from {h(x) |0 ≤ x ≤ J} as h(x) > 0 in concrete local maximum values h'(x) = h(x) − h(x −1), for 1≤ x ≤ J s same in global minima values in h(x) is represented as,

$$h'(x) = h(x) - h(x(y)-1), for\ 1 \le x \le j \quad (17)$$

To group the equalized variance measures(x_i), are differ from the equation

$|h'(x)| < \max|h'(x(y)-1)|$, and | h'(x) |< min{| h'(x −1) |,| h'(x +1) |} (3) h'(x −1) > 0, h'(x +1) < 0 (4) (18)

The histogram feature difference is maximum and minimum where 0 ≤ xi ≤ J, 0 ≤ i ≤ Nmax and Nmax h(xi). So threshold T at an appearance in the modified histogram hmod(x) be created as,

$$h_{mod}(x,y) = \begin{cases} h(x), for\ h(x) \le T \\ T, otherwise \end{cases} \quad (19)$$

After attaining the PDF $h_{mod}(x)$ with cumulative level c(x), it is strong-minded from this representation. Lastly, the conversion function, f(x), is assumed by calculation,

$$f(x) = \left\lfloor \frac{(L-1).c(x)}{c(L-1)} \right\rfloor \quad (20)$$

It has been used successfully for infrared imaging. This method successfully enhances the main object and suppresses the background. The T threshold, although automatically selected, is still not optimal. It chooses the Threshold from only one side of the histogram. The average point in the image histogram is

Doi : https://doi.org/10.54216/JCIM.140203
Received: January 19, 2024 Revised: March 01, 2024 Accepted: June 07, 2024

divided into two segments based on that point. After that, a histogram smoothing function is applied to each segment. There are two aggregate supply functions for two variant segments.

Gray level r_k underneath the regular argument is keen to differentiate the grey levalS_k as inequality can be realized.

$$S_k = (L_1) \times C_1(r_k) \quad \text{and} \quad C_1(r_k) = \left(\sum_{i=0}^{k} n_i\right) \Big/ \left(\sum_{j=0}^{L-1} n_j\right) \tag{21}$$

$$k = 0,1, \dots \dots, L_1$$

To compute the mean distance of gray level cooccurrence in histogram variance L_1 at average weight is processed by,

$$L_1 = \sum_{k=0}^{L-1} P(r_k) * r_k \tag{22}$$

The mean rate of gray level cooccurrence is S_k is represented as, average point Gray level (r_k) be computed as,

$$S_k = (L - 1 - L_1) \times C_2(r_k) + L_1 \tag{23}$$

$$C_2(r_k) = \left(\sum_{i=L_1+1}^{k} n_i\right) \Big/ \left(\sum_{j=L_1+1}^{L-1} n_j\right) \tag{24}$$

$$k = L_1 + 1, \dots \dots, L - 1$$

The image is organized with object difference by handling the probability density function (PDF) according to the following equation.

$$P_{new} = \begin{cases} P_{max} & P(k) = P_{max} \\ \left(\frac{P(k)}{P_{max}}\right)^r \times P_{max} & 0 < P(k) < P_{max} \\ 0 & P(k) = 0 \end{cases} \tag{25}$$

The maximum represented PDF representation image contained cells probably finds the equivalent ratio from 0<r<1 in the best case to manipulate the P_{max}. The image containing cells is varied by grouping the object count based on the cell variation.

The state of best-case difference in 'r' by intending to derive from equation 3, we get isolated difference enhancement.

$$PixDis = \frac{1}{N_{Pix}(N_{Pix}-1)} \sum_{i=0}^{L-2} \sum_{j=i+1}^{L-1} H(i)\, H(j-i) \tag{26}$$

$$for\ i, j \in [0, L-1]$$

The grayscale intensity differs from cell variance. The histogram normalizes the range of grayscale level occurrence to deviate the difference from the variation in the object and its entities. To get the difference by Appling the above equation in the interpretation [0, L-1] histogram is equalized in H (.) with a difference.

3.4 Invariant Entity Scalar Feature Selection (IESFS)

This selects the essential features based on the marginal threshold values. Feature selection reduces the dimensionality nature of non-important features in microscopic images. This chooses the importance of the object segments containing entity values like cell count, colour variants, cell difference, structural principles weights region growing cell. Invariant extracts the feature levels by scaling the variance of difference value to identify the exact features. Selecting these entity-level scalar features improves the classification accuracy due to low dimension microscopic workspace. The convolution Lauer is iterated

Doi : https://doi.org/10.54216/JCIM.140203
Received: January 19, 2024 Revised: March 01, 2024 Accepted: June 07, 2024

based on the sliding window in each convoluted layer by object covering the cell regions in cluster group respectively on all type definition in microscopic images.

At first, we will set an initialization window size tij ×tij for

The first pixel (i, j) is like the standard algorithm, so the window $w_{ij}$is, which is represented by

$$w_{ij} = \{(a,b)|i - t_{ijh} \leq a \leq i + t_{ijh}, j - \leq b \leq j + t_{ijh}\} \quad (27)$$

Where $t_{ijh} = 1 + 2t_{ijh}$.through the Gabor filter, the matrix can be described as:

$$Gw_{ij} = \begin{bmatrix} g(-t_{ijh} - t_{ijh}) & \cdots & g(-t_{ijh}, t_{ijh}) \\ \vdots & \ddots & \vdots \\ g(t_{ijh}, -t_{ijh}) & \cdots & g(-t_{ijh}, t_{ijh}) \end{bmatrix}_{t_{ij} \times t_{ij}} \quad (28)$$

Among the pixels inw_{ij} , we use x_{ij}, and the object covers cell boundary regional, which means the entities and their features weights based on the window size.

$$x_{ij} = \{(a,b) \in w_{ij} | a = i - t_{ijh}$$

Or $a = i + t_{ijh}\ or\ b = j - t_{ijh}\ or\ b = j + t_{ijh}\}$ (29)

i.e., $x_{ij} = 4(t_{ij} - 1)$, is the average defined rate in referred as,

$$m_{ij} = \frac{1}{4(t_{ij}-1)} \quad (30)$$

The variance is:

$$\sigma_{ij} = \frac{1}{4(t_{ij}-1)} \sum_{(a,b) \in x_{ij}} (y(a,b) - m_{ij})^2 \quad (31)$$

And the diffusivity K is given by

$$K_{ij} = \sigma_{ij}/m_{ij} \quad (32)$$

So the larger isK_{ij}, the more severely the image changes 10 equ. The window size will be migrated based on the cell type definition

$$t_{(i,j+1)h} = \begin{cases} \min\ [t_{ijh} + 1, t_{max}]\ \ if\ K_{ij} \leq\ K_T \\ \max[t_{ijh} - 1, t_{min}]\ \ \ if\ K_{ij} > K_T \end{cases} \quad (33)$$

At the maximum and minimum Threshold, window levels are determined by $t_{min}\ and\ t_{max}$ at covered cell types, respectively. Based on the K_T feature threshold margin, the sliding feature weight obtained by window size depends on the differentiated cell types. Each cell type gets grouped into clusters forming threshold values as feature sets.

3.5 Deep Spectral Convolution Neural Network (DSCNN)

To categorize the leukemia types and establish the class, the chosen features are trained in a DSCNN using an optimal liner softmax function and a logical activation function. An improved scalar classifier, the Deep Spectral Convolution Neural Network uses a decision feed forward classification model. Using spectral values obtained from the scaled values of feature threshold margins, the convolution layers are marginalized. In order to degrade the pooling layer and learn feature weights, extended 16 * 16 iteration training is used. Each layer counts the cells using match-case scaled features subsequent to cell segmentation. In order to predict cancer-affected cells, approach utilized a logical activation function to reach the Relu soft max stated function.

Algorithm

Doi : https://doi.org/10.54216/JCIM.140203
Received: January 19, 2024 Revised: March 01, 2024 Accepted: June 07, 2024

Input: Feature SampleFs, Improved feature rule $N_{i(t)} \longrightarrow If$

Output: Optimized class feature

Step 1: Determine the feature weights' maximum weight and rate.

Step 2: Analyze the Fs data and the values in the If dataset.

For every class of layer (CFS)

Step 3: As the feature class (w), ascertain the hidden layer neuron's weight.

$$\int_{i=1}^{size(IF)} \sum If(fs).class = w$$

Nearest feature value (CFS) = nearest feature (WFC)

Every value f for every closest value in the impact ratio's relative relationship
Step 4: Considering the likelihood of the Max feature's grouping, similarity characteristics are categorized.

Feature selection $WFs = \frac{\int_{x=1}^{size(f)} \sum f(w)==fs(w)}{size(f)}$

End

Calculate increasing rate $WFs = \frac{\sum_{i=1}^{size(fw)} cfs}{size(fw)}$

End

Optimized the Computed Malicious Detection (CMD) = wfc return set maximum values

Step 5: Stop

Neural weights indicating the class are assigned to the input features once they have been trained on the classifier structure. By using hidden neurons to learn related traits, the input components aid in the segmentation of sections. To increase classification accuracy by reference, an activation function modifies every neuron. To increase classification accuracy, DSCNN uses a class of feature weights to classify the microscopic pictures according to risk. This lowers the error rate, false rate, and temporal complexity while increasing precision, recall, and f-measure.

4. Materials Used

In this research, we collected a haematological- WBC blood sample dataset for Leukemia cancer identification. Dataset name: ASH-(The American Society of Hematology).Repository: Kaggle (Legally licensed benchmark dataset) Link availability: www.kaggle.com/paultimothymooney/blood-cells and https://homes.di.unimi.it/scotti/all/ ASH is a collective haematology patient's blood sample dataset.

Doi : https://doi.org/10.54216/JCIM.140203
Received: January 19, 2024 Revised: March 01, 2024 Accepted: June 07, 2024

Features considered: shape projection, Hausdorff's Dimension, colour features, Histogram features, statics segment features, grey level features, cooccurrence features, cell counts, and spatial entity count. Cell Difference features neutrophils, lymphocytes, monocyte, basophil, platelet, CBC, and Erythrocytes. The blood samples are collected from the periodic difference on microscopic images and observed manually on the blood sample on the microscope.

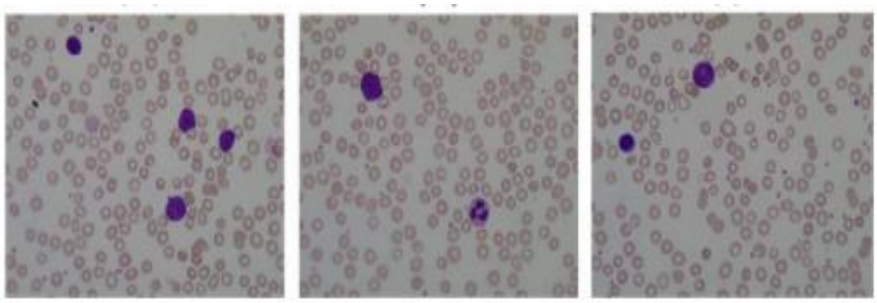

Figure 4: ASH-Dataset ALL_IDB1

The ASH images from the WBC blood bank are a benchmark dataset that includes leukemic and standard microscopic blood photographs. The database consists of 3000 images, including the 3:1 of test and train samples.

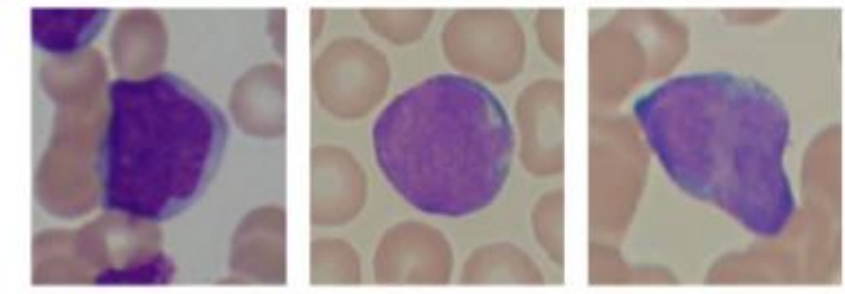

Figure 5: ASH-Dataset ALL_IDB2

Reference Dataset Types: ALL-IDB1, ALL-IDB2, Blood Seg, Cella vision, SMC-IDB etc., contains WBC microscopic image collections dataset. The dataset images are from sliced windows ranging 120*120 Pixels with coloured images containing the intensity of Leukemia features. This group of clipped normal and blast cell area of interest is a part of the ALL-IDB1 dataset. With the exception of image size, ALL-IDB2 photos are comparable to ALL-IDB1 images in terms of their grey-level characteristics. The suggested algorithm was estimated using the following parameters: time complexity performance, MSE, PSNR, F1 score, sensitivity, specificity, and accuracy of classification. Two prior algorithms are compared with the proposed Deep Vectorized Scaling Neural Network (DVSNN) algorithm: the Adaptive Neuro-Fuzzy (ANF) method and the Dense Convolutional Neural Network (DCNN).

Table 1: Details of simulation parameters

Parameters	Values
Tool	Matlab 2017a
Name of the dataset	ASH-(The American Society of Hematology)
Training image	350

Doi : https://doi.org/10.54216/JCIM.140203
Received: January 19, 2024 Revised: March 01, 2024 Accepted: June 07, 2024

Testing image	150

Table 1 displays the simulation parameters in detail. A confusion matrix is used to assess all the factors in order to calculate the F1 measure, sensitivity, and specificity.The percentage of real positive readings that correctly diagnosed leukemia malignancy is measured by sensitivity (Se). The computed equation is written like this:

$$\text{Sensitivity (Se)} = \frac{t_p}{t_p + f_n} * 100 \quad (34)$$

Assume that t_p stands for actually positive values and f_n for falsely negative values obtained from microscopic images.

Result and Discussion

Table 2: Comparison of different filters

Different Parameters	Different Filters	Response (dB)
MSE (dB)	Gaussian Filter	18.42
	Mean Filter	13.14
	Median Filter	9.25
	Adaptive wiener filter	9.13
MAE (dB)	Gaussian Filter	0.0688
	Mean Filter	0.0525
	Median Filter	0.0430
	Adaptive wiener filter	0.0380
PSNR(dB)	Gaussian Filter	34.20
	Mean Filter	34.51
	Median Filter	42.02
	Adaptive wiener filter	48.21

Table 3: Comparison of segmentation with response parameter

Different Parameters	Different Segmentation	Response (dB)
Global Consistency Error(dB)	K-means Clustering	0.581

Doi : https://doi.org/10.54216/JCIM.140203
Received: January 19, 2024 Revised: March 01, 2024 Accepted: June 07, 2024

	Fuzzy C Means Clustering	0.522
	IESFS-DSCNN	0.326
DICE Coefficient	K-means Clustering	0.64
	Fuzzy C Means Clustering	0.61
	IESFS-DSCNN	0.99

Table 4: Analysis of Sensitivity performance

Number of microscopic images	ANF in %	DCNN in %	DVSNN in %	IESFS-DSCNN
100	55	61	72	89.6
200	61	66	78	91.2
300	67	72	82	92.1
400	71	76	86	92.7

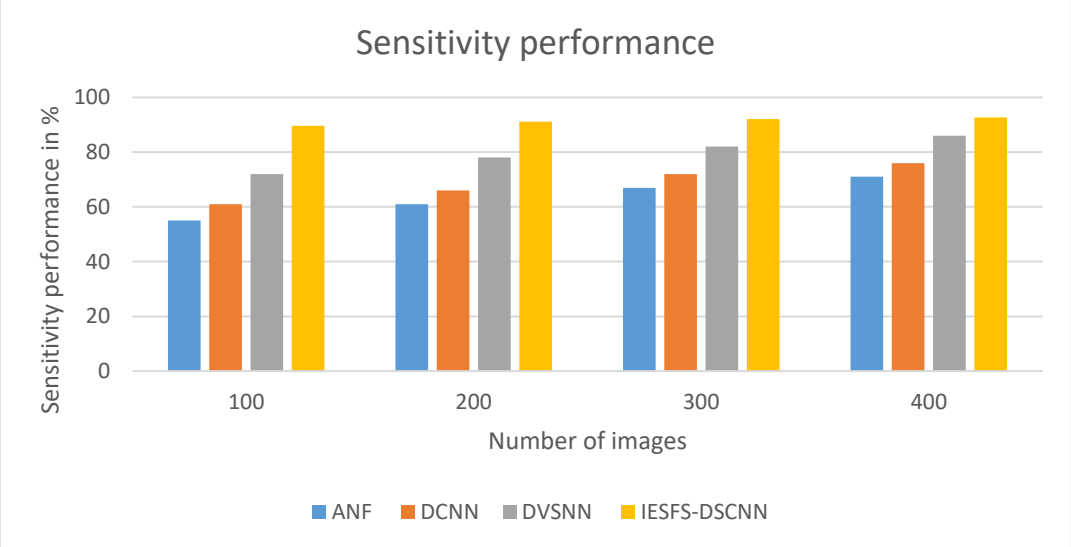

Figure 6: Analysis of Sensitivity performance

Sensitivity (Se) performance for leukemia malignancy identification is shown in Figure 6 and Table 4. Compared to the recommended IESFS-DSCNN, the Deep Vectorized Scaling Neural Network (DVSNN) algorithm performs 86% better in terms of sensitivity (Se). Comparably, the results of the current algorithm demonstrate that, in terms of Sensitivity (Se), the ANF approach performs 71%, while the DCNN technique performs 76%.

Doi : https://doi.org/10.54216/JCIM.140203
Received: January 19, 2024 Revised: March 01, 2024 Accepted: June 07, 2024

$$Specificity\ (Sp) = \frac{t_n}{t_n + f_p} * 100 \quad (35)$$

The calculation of specificity (S_p) is represented by the above equation. Assume that t_n stands for true negative values and false-positive values (fp) are derived from pictures of microscopic objects.

Table 5: Analysis of Specificity performance

Number of microscopic images	ANF in %	DCNN in %	DVSNN in %	IESFS-DSCNN
100	54	60	70	88.9
200	60	67	77	90.5
300	65	71	80	91.9
400	72	75	85	92.3

An examination of Specificity performance is shown in Table 5. The Specificity of leukemia cancer microscopic photos calculates the proportion of correctly identified negative values.

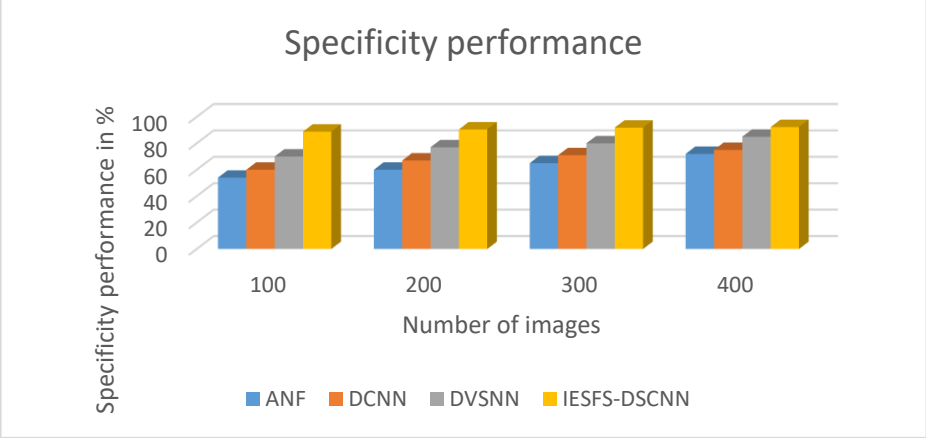

Figure 7: Analysis of Specificity (Sp) performance

Figure 7 compares the Specificity (Sp) performance of earlier methods with leukaemia cancer detection. Specificity (Sp) performance of the suggested DVSNN algorithm is 85%. The current algorithm yields a performance result of 75% for the DCNN method and 65% for the ANF algorithm in terms of Specificity (Sp).

$$F1\ score = 2\left(\frac{SeXSp}{Se+Sp}\right) \quad (36)$$

The f1-score performance is computed using the equation above.

Doi : https://doi.org/10.54216/JCIM.140203
Received: January 19, 2024 Revised: March 01, 2024 Accepted: June 07, 2024

Table 6: Analysis of F1- score performance

Number of microscopic images	ANF in %	DCNN in %	DVSNN in %	IESFS-DSCNN
100	56.2	61.3	71.4	86.4
200	62.1	68.6	77.1	91.1
300	66.4	72.1	81.6	92.2
400	73.7	77.2	87.5	93.6

Table 6 shows an analysis of the proposed algorithm's f1 score performance in comparison to the findings of prior algorithms. When compared to other approaches, the suggested algorithm performs well.

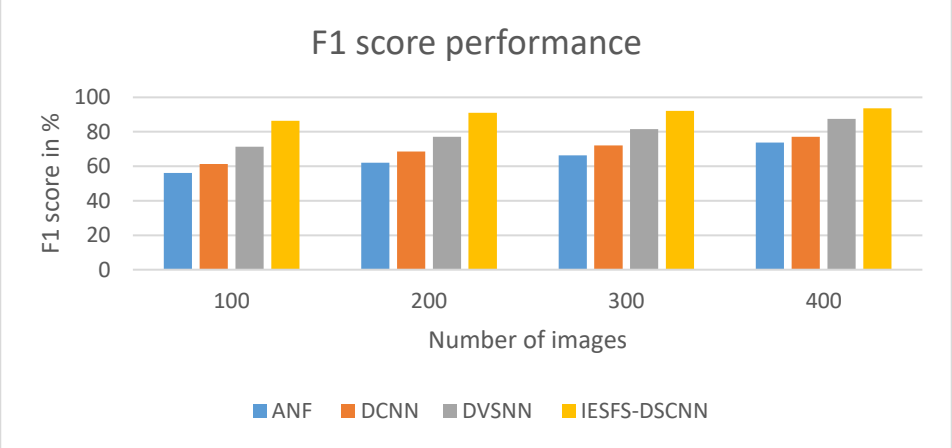

Figure 8: Analysis of F1-score performance

The f1 score performance for leukaemia cancer detection is defined in Figure 8. The performance result for the F1 score of the proposed algorithm is 87.5%. Comparably, the f1-score performance of the current algorithms is 73.7% for the ANF algorithm and 77.2% for the DCNN algorithm. The classification accuracy performance is determined using the equation below.

$$\text{Classification accuracy performance} = \frac{t_p+t_n}{t_p+t_n+F_p+F_n} * 100 \quad (37)$$

Table 7: Analysis of Classification accuracy performance

Number of microscopic images	ANF in %	DCNN in %	DVSNN in %	IESFS-DSCNN

Doi : https://doi.org/10.54216/JCIM.140203
Received: January 19, 2024 Revised: March 01, 2024 Accepted: June 07, 2024

100	57	62	73	88.2
200	63	69	78	91.7
300	67	73	82	93.9
400	75	78	89	94.8

Table 7 displays an analysis of accuracy performance comparative data. The accuracy is calculated by dividing the total number of cases that were precisely identified based on how many test microscopic images correctly represented the overall performance.

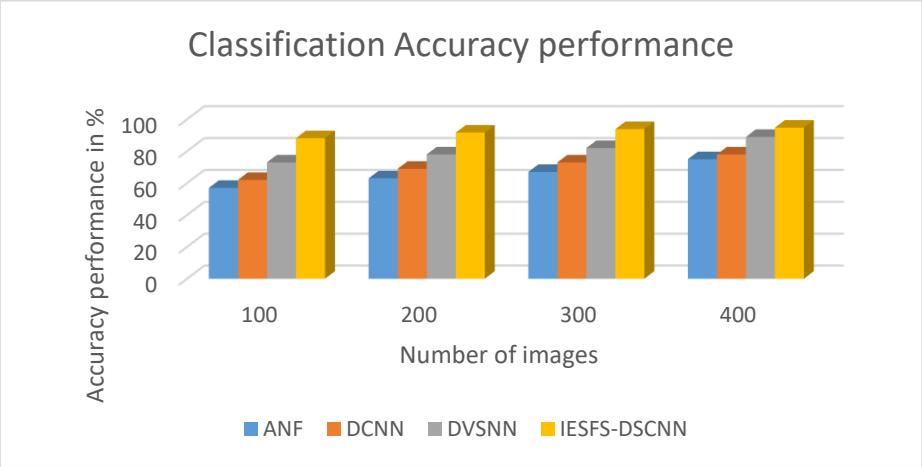

Figure 9: Analysis of Classification Accuracy performance

The results of a comparison of the suggested and current algorithms' performance in terms of classification accuracy are shown in Figure 9. When compared to DVSNN, the suggested IESFS-DSCNN algorithm performs 89% better in terms of classification accuracy. Comparably, the accuracy performance of the current algorithm is 78% for the DCNN algorithm and 75% for the ANF classification algorithm.

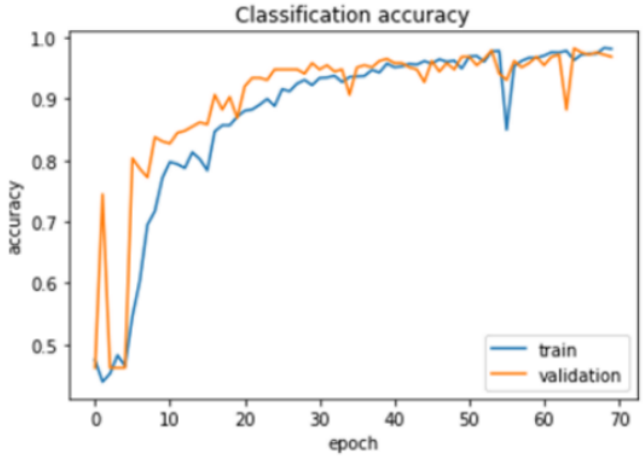

Figure 10: classification accuracy train and validation performance

Doi : https://doi.org/10.54216/JCIM.140203
Received: January 19, 2024 Revised: March 01, 2024 Accepted: June 07, 2024

Using features from the darknet-IoT23 dataset, Figure 12 explains risk level identification for IoT traffic detection in cyber security. In order to enhance the standard features and decrease the risk features, the suggested method, IESFS-DSCNN, computed risk level 12.67%, low risk 11.34%, and average level 75.14% utilizing the maximum weighted feature. While DCNN is analyzed standard 67.14%, low-risk at 29.22%, and risk 15.32%, previous methods of DVSNN evaluate the predicted 70.12%, low-risk at 15.89%, and risk at 13.42%. According to ANF, the danger is 16.01, the low-risk level is 30.61%, and the normal is 60.19%.

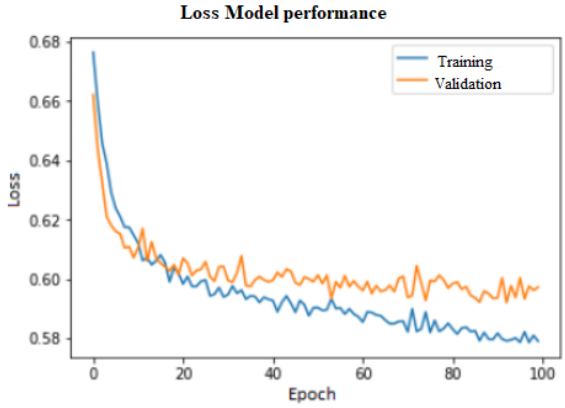

Figure 11: Loss model performance

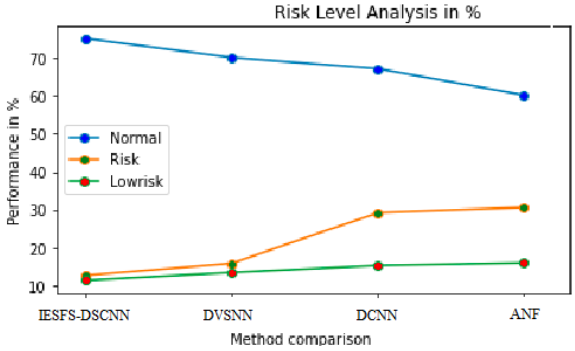

Figure 12: Analysis of Multi-Scale Features Risk Level

$$\text{Time complexity (Tc)} = \frac{i*(i-1)}{Total\ processing\ time} \quad (38)$$

where i stand for the quantity of example pictures.

Doi : https://doi.org/10.54216/JCIM.140203
Received: January 19, 2024 Revised: March 01, 2024 Accepted: June 07, 2024

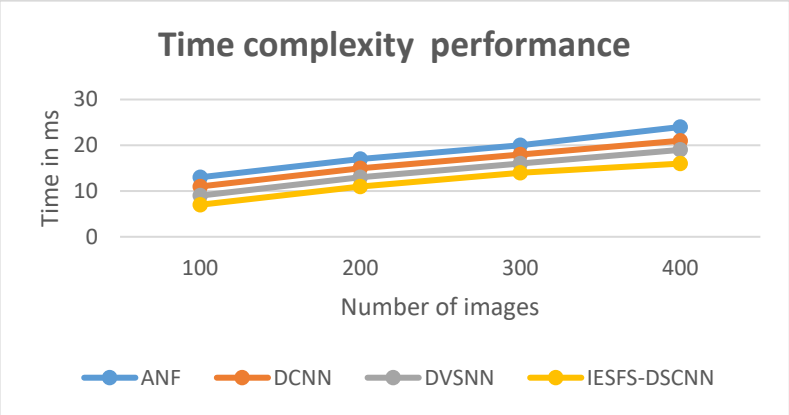

Figure 13: Analysis of time complexity performance

The investigation of the time complexity performance for leukemia cancer diagnosis in milliseconds is shown in Figure 13 above. The suggested IESFS-DSCNN algorithm performs 19 ms faster in terms of time complexity than the DVSNN approach. According to the current algorithmic conclusion, the DCNN algorithm performs with a time complexity performance of 21 ms, while the ANF method performs with a time complexity performance of 24 ms. Compared to existing approaches, the concept offers a shorter time frame for leukemia cancer detection.

6. Conclusion

In conclusion, this research presents a Deep Spectral Convolution Neural Network Based Leukemia Cancer Detection Using Invariant Entity Scalar Feature Selection method for leukaemia cancer detection. Boundaries and similar features are thought to be shape features in the leukemia-affected area, increasing the accuracy of identification. After gathering the suggested tiny blood cell image dataset, the pictures were cleaned up to remove noise and their shape was modified using adaptive median filters. Lastly, the suggested algorithm successfully categorizes the risk of cancer from leukemia. The suggested algorithm yields outcomes. The results show that the performance in terms of sensitivity (Se) is 92.1%, specificity (Sp) is 91.3%, f1 score is 87.5%, classification accuracy is 92.7%, and time complexity is 19 ms. When compared to alternative techniques, the suggested IESFS-DSCNN algorithm performs well in terms of temporal complexity, f1-score, sensitivity, specificity, and classification accuracy.

References

[1] D. Kumar et al., "Automatic Detection of White Blood Cancer From Bone Marrow Microscopic Images Using Convolutional Neural Networks," in IEEE Access, vol. 8, pp. 142521-142531, 2020, DOI: 10.1109/ACCESS.2020.3012292.

[2] S. O. Heriawati, T. Harsono, M. M. Bachtiar and Y. Hernaningsih, "Blood Cells Classification for Identification of Acute Lymphoblastic Leukemia on Microscopic Images Using Image Processing," 2021 International Electronics Symposium (IES), 2021, pp. 215-220, DOI: 10.1109/IES53407.2021.9593939.

[3] N. S. P. Kong, H. Ibrahim, C. H. Ooi and D. C. J. Chieh, "Enhancement of Microscopic Images Using Modified Self-Adaptive Plateau Histogram Equalization," 2009 International Conference on Computer Technology and Development, 2009, pp. 308-310, DOI: 10.1109/ICCTD.2009.46.

[4] H. Li, X. Zhao, A. Su, H. Zhang, J. Liu and G. Gu, "Color Space Transformation and Multi-Class Weighted Loss for Adhesive White Blood Cell Segmentation," in IEEE Access, vol. 8, pp. 24808-24818, 2020, DOI: 10.1109/ACCESS.2020.2970485.

[5] M. H. Waseem et al., "On the Feature Selection Methods and Reject Option Classifiers for Robust Cancer Prediction," in IEEE Access, vol. 7, pp. 141072-141082, 2019, DOI: 10.1109/ACCESS.2019.2944295.

Doi : https://doi.org/10.54216/JCIM.140203
Received: January 19, 2024 Revised: March 01, 2024 Accepted: June 07, 2024

[6] Ambeth Kumar, V.D. (2017). Automation of Image Categorization with Most Relevant Negatives. Pattern Recognition and Image Analysis, 27(3), 371–379.
[7] Kumar, I., Kumar, A., Kumar, V.D.A. et al. (2022) Dense Tissue Pattern Characterization Using Deep Neural Network. Cogn Comput 14, 1728–1751.
[8] L. KG and N. Manja Naik, "Automated Detection of White Blood Cells Cancer Disease," 2019 1st International Conference on Advances in Information Technology (ICAIT), 2019, pp. 24-28, DOI: 10.1109/ICAIT47043.2019.8987352.
[9] R. P and S. D. P, "Detection of Blood Cancer-Leukemia using K-means Algorithm," 2021 5th International Conference on Intelligent Computing and Control Systems (ICICCS), 2021, pp. 838-842, DOI: 10.1109/ICICCS51141.2021.9432244.
[10] Ambeth Kumar, S. Malathi ,R. Venkatesan, K Ramalakshmi, Weiping Ding, Abhishek Kumar. (2020). Exploration of an innovative geometric parameter based on performance enhancement for foot print recognition. Journal of Intelligent and Fuzzy System , 38 (2), 2181-2196.
[11] V. Acharya, V. Ravi, T. D. Pham and C. Chakraborty, "Peripheral Blood Smear Analysis Using Automated Computer-Aided Diagnosis System to Identify Acute Myeloid Leukemia," in IEEE Transactions on Engineering Management, DOI: 10.1109/TEM.2021.3103549.
[12] A. Soleimanian et al., "An Efficient Graphene Quantum Dots-Based Electrochemical Cytosensor for the Sensitive Recognition of CD123 in Acute Myeloid Leukemia Cells," in IEEE Sensors Journal, vol. 21, no. 15, pp. 16451-16463, 1 Aug.1, 2021, DOI: 10.1109/JSEN.2021.3079224.
[13] D. Kumar et al., "Automatic Detection of White Blood Cancer From Bone Marrow Microscopic Images Using Convolutional Neural Networks," in IEEE Access, vol. 8, pp. 142521-142531, 2020, DOI: 10.1109/ACCESS.2020.3012292.
[14] Kumar, V.D.A., Sharmila, S., Kumar, A. et al. (2023). A novel solution for finding postpartum haemorrhage using fuzzy neural techniques. Neural Comput & Applic. 35(33), 23683–23696
[15] L. Boldú, A. Merino, S. Alférez, A. Molina, A. Acevedo, and J. Rodellar, ‘‘Automatic recognition of different types of acute leukaemia in peripheral blood by image analysis,’’ J. Clin. Pathol., vol. 72, no. 11, pp. 755–761, Nov. 2019.
[16] A. Shah, S. S. Naqvi, K. Naveed, N. Salem, M. A. U. Khan and K. S. Alimgeer, "Automated Diagnosis of Leukemia: A Comprehensive Review," in IEEE Access, vol. 9, pp. 132097-132124, 2021, DOI: 10.1109/ACCESS.2021.3114059.
[17] P. K. Das, S. Meher, R. Panda and A. Abraham, "An Efficient Blood-Cell Segmentation for the Detection of Hematological Disorders," in IEEE Transactions on Cybernetics, DOI: 10.1109/TCYB.2021.3062152.
[18] D. Kumar et al., "Automatic Detection of White Blood Cancer From Bone Marrow Microscopic Images Using Convolutional Neural Networks," in IEEE Access, vol. 8, pp. 142521-142531, 2020, DOI: 10.1109/ACCESS.2020.3012292.
[19] Hemamalini, Selvamani, and Visvam Devadoss Ambeth Kumar. (2022). Outlier Based Skimpy Regularization Fuzzy Clustering Algorithm for Diabetic Retinopathy Image Segmentation. Symmetry, 14(12), 2512
[20] T. Dharani and S. Hariprasath, "Diagnosis of Leukemia and its types Using Digital Image Processing Techniques," 2018 3rd International Conference on Communication and Electronics Systems (ICCES), 2018, pp. 275-279, DOI: 10.1109/CESYS.2018.8724075.
[21] Balakrishnan, Chitra, and V. D. Ambeth Kumar. (2023). IoT-Enabled Classification of Echocardiogram Images for Cardiovascular Disease Risk Prediction with Pre-Trained Recurrent Convolutional Neural Networks. Diagnostics 13(4), 775
[23] S. Khan, M. Sajjad, T. Hussain, A. Ullah and A. S. Imran, "A Review on Traditional Machine Learning and Deep Learning Models for WBCs Classification in Blood Smear Images," in IEEE Access, vol. 9, pp. 10657-10673, 2021, DOI: 10.1109/ACCESS.2020.3048172.
[24] J. Amin et al., "An Integrated Design based on Dual Thresholding and Features Optimization for White Blood Cells Detection," in IEEE Access, DOI: 10.1109/ACCESS.2021.3123256.
[25] H. N. Fakhouri and S. H. Al-Sharaeh, "A hybrid methodology for automation the diagnosis of leukaemia based on quantitative and morphological feature analysis," Modern Appl. Sci., vol. 12, no. 3, p. 56, Feb. 2018.

Doi : https://doi.org/10.54216/JCIM.140203
Received: January 19, 2024 Revised: March 01, 2024 Accepted: June 07, 2024

[26] Piyush K. Pareek, Pixel Level Image Fusion in Moving objection Detection and Tracking with Machine Learning ",Fusion: Practice and Applications, Volume 2 , Issue 1 , PP: 42-60, 2020
[27] Shivam Grover, Kshitij Sidana, Vanita Jain, "Egocentric Performance Capture: A Review", Fusion: Practice and Applications, Volume 2, Issue 2 , PP: 64-73, 2020.
[28] Abdel Nasser H. Zaied, Mahmoud Ismail and Salwa El- Sayed, A Survey on Meta-heuristic Algorithms for Global Optimization Problems, Journal of Intelligent Systems and Internet of Things,Volume 1 , Issue 1 , PP: 48-60, 2020
[29] Mahmoud H.Alnamoly, Ahmed M. Alzohairy, Ibrahim M. El-Henawy, "A survey on gel images analysis software tools, Journal of Intelligent Systems and Internet of Things,Volume 1 , Issue 1 , PP: 40-47, 2021.
[30] Sherubha, "Graph Based Event Measurement for Analyzing Distributed Anomalies in Sensor Networks", Sådhanå(Springer), 45:212, https://doi.org/10.1007/s12046-020-01451-w

Doi : https://doi.org/10.54216/JCIM.140203
Received: January 19, 2024 Revised: March 01, 2024 Accepted: June 07, 2024